ISSN 1606-867X (Print)
ISSN 2687-0711 (Online)
Condensed Matter and Interphases
Kondensirovannye Sredy i Mezhfaznye Granitsy
https://journals.vsu.ru/kcmf/

Review

Review article
https://doi.org/10.17308/kcmf.2025.27/12763

Graphitic carbon nitride: properties and applications in gas sensing. Review

C. D. Bui[1]✉, S. S. Nalimova[1], V. T. A. Nguyen[2]

[1]Saint Petersburg Electrotechnical University «LETI»,
5 ul. Professora Popova, Saint Petersburg 197022, Russia Federation

[2]Peter the Great St. Petersburg Polytechnic University,
29 ul. Politekhnicheskaya, Saint Petersburg 195251, Russia Federation

Abstract

Purpose: Nowadays gas sensors are of great interest for disease detection and assessment of treatment efficacy based on exhaled breath analysis. One of the promising materials for gas sensors are composites of graphitic carbon nitride with metal oxides.

Experimental: The article considers the basic properties of g-C_3N_4 and provides a review of methods that can be effective for obtaining its composites with metal oxides.

Conclusions: The study presents the mechanism of interaction of g-C_3N_4 with gases of different nature. In addition, it gives some examples of sensors based on composites of g-C_3N_4 with metal oxides.

Keywords: Graphitic carbon nitride, Gas sensing, Nanocomposites

For citation: Bui C. D., Nalimova S. S., Nguyen V. T. A. Graphite carbon nitride: properties and applications in gas sensing. Review. *Condensed Matter and Interphases*. 2025;27(2): 177–189. https://doi.org/10.17308/kcmf.2025.27/12763

Для цитирования: Буй К. Д., Налимова С. С., Нгуен В. Т. А. Графитоподобный нитрид углерода: свойства и применение в газовой сенсорике. Обзор. *Конденсированные среды и межфазные границы*. 2025;27(2): 177–189. https://doi.org/10.17308/kcmf.2025.27/12763

✉ Bui Cong Doan, e-mail: congdoan6997@gmail.com

1. Introduction

Gas sensors are widely used to detect low concentrations of flammable, explosive or toxic gases and to monitor environmental pollution. Generally, the main requirements for a gas-sensitive material are as follows: high sensitivity, fast performance and good selectivity. Development of inexpensive and reliable sensor devices for gas detection, especially at room temperature, is an important scientific and technological task. For its solution, sensors operating on the basis of various principles are used. In regard to this, semiconductor adsorption sensors are favorably characterized by simple construction, low cost and a wide choice of materials of the primary sensing element [1, 2]. The principle of their operation is based on the change in the resistance of the material when chemical reactions of interaction with oxidizing or reducing gases occur on its surface [3, 4]. The sensing material should be selected so that it has a large surface available for interaction with gas molecules, suitable active centers for their adsorption. The main advantage of semiconductor gas sensors is their high sensitivity, but their wide application is limited by low selectivity and high operating temperatures [5]. The problems of selectivity can be solved by using different sensitive materials and realizing multisensor systems [6], as well as thermomodulation mode [7, 8]. To reduce operating temperatures, heating is replaced by exposure to ultraviolet or visible light [9, 10]. Over the years, the gas-sensitive properties of *n*-type semiconductor oxides such as SnO_2 [11], ZnO [12], TiO_2 [13], Fe_2O_3 [14] и WO_3 [15] have been widely studied. To a lesser extent, p-type oxides such as CuO [16], NiO [17] и Co_3O_4 [18] have also been investigated. Studies on mixed metal oxides (perovskites [19] and cubic spinels, such as ferrites [20] and orthostannates [21]), have shown that they can have much higher response in some cases. In the last decade, two-dimensional (2D) materials [22] with nanoscale thickness and large surface-to-volume ratio have shown great promise for gas sensors. Efficient gas sensors can be obtained by combining the advantages of different groups of materials and creating composites of metal oxides with 2D materials [23, 24].

Nanomaterials based on graphitic carbon nitride (g-C_3N_4) have found wide applications in various types of catalysis due to their low density, high chemical stability, tunable morphology and low consumption [25]. The g-C_3N_4 has a hierarchical structure and consists of an aromatic plane and a π-conjugated s-triazine unit composed of hybridized multiple sp, sp^2 and sp^3 carbon and nitrogen atoms [26].

These materials are usually fabricated by thermal condensation of nitrogen-containing precursors such as melamine, dicyandiamide and urea [27, 28]. The morphology of g-C_3N_4 can be easily controlled, which allows increasing the specific surface area and the number of adsorption centers for reactions with target gases.

Based on the mechanism of gas sensitivity, the large specific surface area and a larger number of adsorption centers in g-C_3N_4 allow more gas molecules to participate in reactions with target gases. In addition, simple and inexpensive methods of obtaining g-C_3N_4 are advantages of its application in the field of gas sensing. Since the band gap of g-C_3N_4 is 2.7 eV, the valence band electrons easily move to the conduction band when exposed to visible light, which leads to excellent catalytic activity and allows reducing the activation energy of the chemical reaction leading to a sensor response.

Nitrogen atoms give g-C_3N_4 semiconducting properties and complexation ability, making it to some extent a more efficient catalyst than graphene. However, some drawbacks remain, limiting its further application in this field. The g-C_3N_4 obtained by direct calcination of the precursor usually has a dense structure and low specific surface area [29]. The low charge carrier mobility and low electrical conductivity of pure g-C_3N_4 result in long response time and poor fast performance [30]. Pure g-C_3N_4 has low sensitivity, high operating temperature and low selectivity [31]. Creating composites of g-C_3N_4 with metal oxides allows increasing the surface area, creating more surface active centers. The formation of a heterojunction between the material and g-C_3N_4 can provide electron transfer. Thus, SnO_2/g-C_3N_4 composites show higher sensitivity and selectivity to ethanol compared to SnO_2 [32]. The g-C_3N_4/ZnO based sensor has been shown to have excellent performance for CH_4 detection [33].

The aim of this study is to analyze the properties of g-C_3N_4, review the main methods of obtaining its composites with metal oxides and the achieved results on their application in gas sensing.

2. The structure of g-C_3N_4

The strong covalent bonding between N and C atoms in the g-C_3N_4 layer provides its high chemical and thermal stability [34]. Two-dimensional π-bonded polymer systems including triazine or tri-s-triazine (s-heptazine) blocks linked by tertiary amines make g-C_3N_4 stable at room temperature (see Fig. 1) [35].

The individual layers are linked to each other by weak van der Waals forces. Under ambient conditions, g-C_3N_4 is thermally and chemically stable, biocompatible, environmentally friendly and resistant to acidic and alkaline environments [36].

The g-C_3N_4 obtained by thermal condensation of N-containing precursors has low crystallinity due to the appearance of defects connected with insufficient deamination during thermal condensation and the formation of heptazine-based melon. In melon, layers of one-dimensional chains of NH-linked melem monomers are connected by hydrogen bonds in a zigzag shape. As a result, the charge carriers generated by photon exposure are concentrated in certain regions, which reduces the conductivity [37].

3. The properties of g-C_3N_4

Graphitic carbon nitride (g-C_3N_4) has recently attracted the interest of researchers due to its outstanding properties including low cost, large surface area, abundance in nature, fast electron transfer, π-π bond pairing, and absence of metals [38]. It is an excellent polymeric semiconductor operating in the visible region of the spectrum, with biocompatibility and excellent catalytic properties.

Pacha et al. synthesized bulk and thin film g-C_3N_4 by thermal polycondensation of melamine [39]. X-ray photoelectron spectroscopy was used to determine the chemical composition of bulk and thin films of g-C_3N_4. Peaks corresponding to C 1*s*, N 1*s*, as well as a peak of O 1*s* of weak intensity, are observed in the spectra (see Fig. 2).

The paper shows the C-V characteristics of the ITO/g-C_3N_4/Al structure from -5 V to 5 V for a wide frequency range from 1 kHz to 1 MHz. At 1 kHz, the capacitance is 3.42 nF, and it decreases to 3.18 nF as the frequency increases up to 100 kHz. The decrease in capacitance at high frequencies can be explained by the low conductivity of g-C_3N_4. Moreover, the paper shows the frequency dependence of dielectric constant of g-C_3N_4 thin film, the values of which are 8.05–7.17 in the frequency range from 100 Hz to 100 kHz.

Giusto et al. observed that g-C_3N_4 film has a refractive index (n_D = 2.43) which is the highest for polymeric materials [40]. The highly oriented and conjugated g-C_3N_4 films exhibit intense blue photoluminescence (PL) under UV excitation. The PL spectra of g-C_3N_4 films differ from those of powders due to the large number of allowed radiative transitions between different energy levels upon light excitation. When the film thickness is more than 1 μm, the absorption spectra are similar to the absorption spectra of

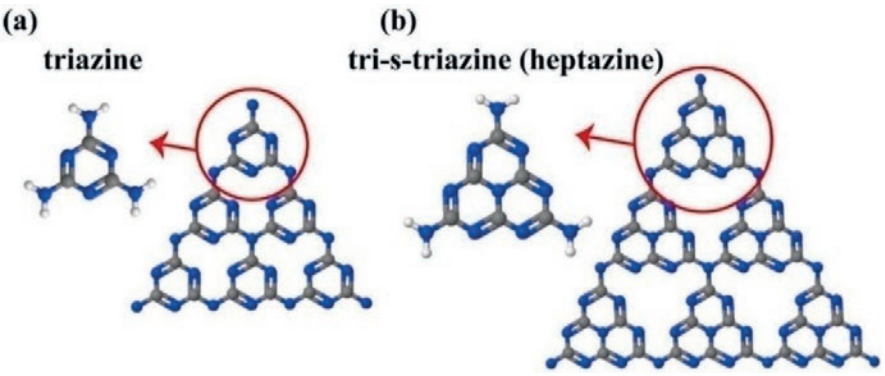

Fig. 1. (a) Triazine and (b) tri-s-triazine (heptazine) two-dimensional network based on g-C_3N_4 (white, gray, and blue balls denote H, C, and N, respectively) [35]

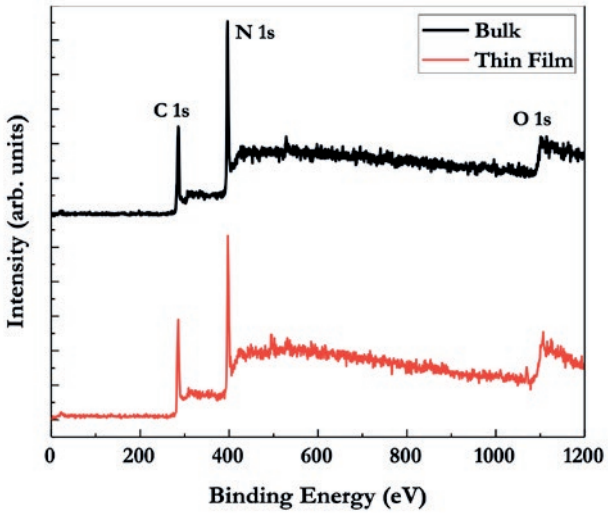

Fig. 2. X-ray photoelectron spectrum of bulk and thin-film g-C_3N_4 [31]

bulk powder. The optical absorption edge shows the thickness dependence of absorption [41].

The absorption spectra of g-C_3N_4 powders show that the absorption edge of the material is around λ = 450 nm [42]. By contrast, g-C_3N_4 films exhibit thickness dependent absorption spectra. A 55 nm thick g-C_3N_4 film exhibits intense absorption bands at λ = 307 nm and two additional bands at λ = 366 and 386 nm; they are due to π-π*, π-π* and LP-π* transitions, respectively, where π* are the levels of excited π-orbitals. The differences between the wavelengths of the calculated and measured absorption bands are related to the size of the monoatomic sheets and the thickness of the films. Theoretical calculations show that the energy bands will be separated into discrete energy levels.

Being a carbon/nitrogen compound with tri-s-triazines linked via tertiary amines, g-C_3N_4 has corresponding band positions (conduction band (CB) at ≈ −1.1 eV and valence band (VB) at ≈+ 1.6 eV relative to the standard hydrogen electrode (NHE) at pH = 0) [43]. The chemical potential allows g-C_3N_4 to exhibit redox properties in various photocatalytic reactions under visible light irradiation. As shown in Fig. 3, the energy conversion process under sunlight in bulk g-C_3N_4 mainly involves four factors, namely, photon excitation, generation/separation of photogenerated charge carriers, and surface redox reactions involving electrons/holes [44].

The disadvantages of bulk g-C_3N_4 are high bulk or surface recombination. It limits the ability of pure g-C_3N_4 to achieve high photocatalytic performance.

To overcome the drawbacks of pure g-C_3N_4, its composites with other materials are prepared and investigated. In particular, composites with metal oxides are used to improve sensor and photocatalytic performance.

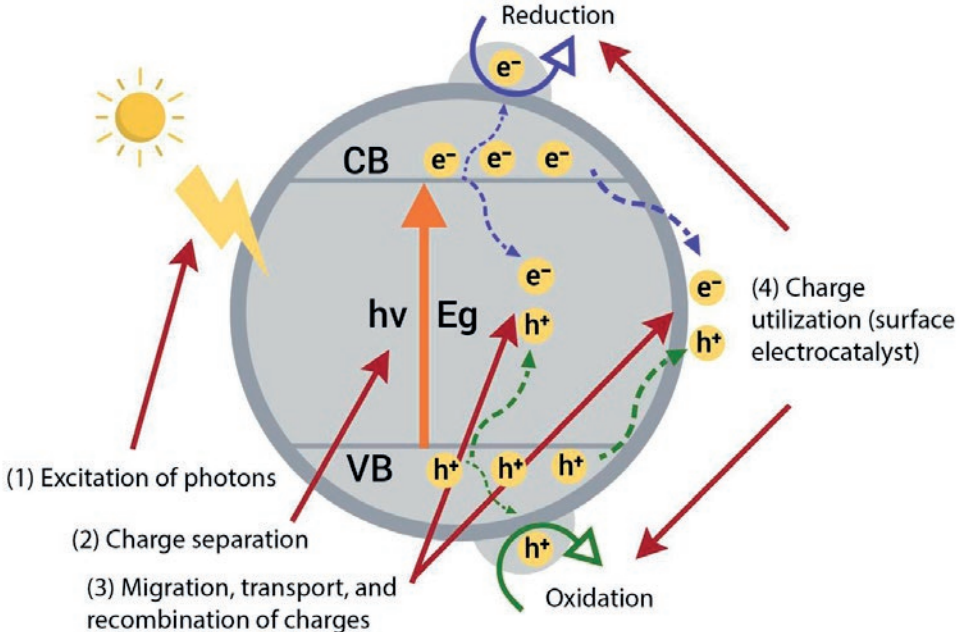

Fig. 3. Four main processes of g-C_3N_4 photocatalysis

4. Synthesis methods of metal oxide composites with g-C_3N_4

The synthesis of g-C_3N_4 composites with various compounds, including TiO_2 [45], ZnO [46], CdS [47], Bi_2WO_6 [48], Bi_2MoO_6 [49], In_2O_3 [50], Ag_3PO_4 [51], AgBr [52] и MoS_2 [53], has been reported in the literature. The heterostructure formed based on g-C_3N_4 cannot be formed with all materials. Since the efficiency of the heterostructure stimulated by visible light depends on the ability to hybridize bonds, the main criteria for material selection are the corresponding band structure. In addition, band bending occurs at the interface due to the potential difference between the semiconductors in contact. The photogenerated electrons and holes move in the opposite directions due to the internal field created by the band bending. As a result, pairs of electrons and holes are effectively separated and combined on the opposite sides of the heterojunction. ultrasonic mixing, precipitation-calcination, ultrasonic dispersion, hydrothermal method, and ultrasonic deposition are the methods for synthesizing g-C_3N_4 composites.

Ultrasonication is the simplest method for producing g-C_3N_4-based composites. The method involves mixing g-C_3N_4 powders (derived from nitrogen-containing precursors such as urea, melamine) with appropriate metals or metal oxides in water or an organic solvent. In this process, it is possible to form composites in which the metal oxide is distributed on the surface of g-C_3N_4 during the stirring process. The nanocomposite is extracted after complete evaporation of the solvent or water during heat treatment. In addition, other factors such as mechanical stirring and particle movement in the ultrasonic field can modify the deposition and dissolution process. A simple precipitation-calcination procedure was used by Yuan et al. [46] to obtain nanocomposites consisting of ZnO on g-C_3N_4 nanosheets (see Fig. 4).

Nanocomposites based on g-C_3N_4 can be obtained by heat treatment at high temperatures (calcination) of metal oxides with g-C_3N_4 precursors. Due to its advantages including low time, low cost, simplicity and high yield, this method is a popular method for fabricating g-C_3N_4-based nanocomposites. However, the obtained composites have small specific surface area, large size particles, inhomogeneous particle distribution, etc., because there is no mixing of precursors in aqueous medium in this method, and higher calcination temperatures are required. The formation of heterostructure between the components in the fabricated nanocomposite reduces the probability of recombination of electron-hole pairs.

The hydrothermal method has become a promising technology for the creation of nanocomposite materials [54]. In this method, the crystallite size, morphology and crystallinity of materials can be improved due to the fact that the process takes place at relatively low temperatures. In addition, there are other parameters such as pressure, reaction temperature, pH, additives, solvent types, reaction time and precursor

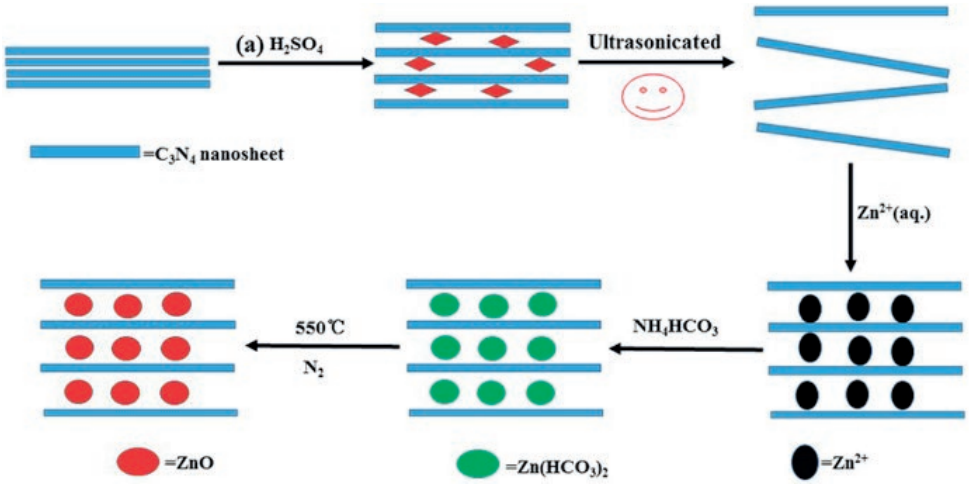

Fig. 4. Fabrication process of nanocomposites from g-C_3N_4 and ZnO nanosheets [46]

composition that determine the surface chemistry and play an important role in the synthesis process. Idresse et al. [55] used the hydrothermal method to form niobium pentoxide (Nb_2O_5)/g-C_3N_4 heterostructure (see Fig. 5).

Due to the low temperature used in this process, the particles obtained by hydrothermal synthesis have higher specific surface area, smaller size and better stability compared to those obtained by solid-state technology.

The synthesis of nanomaterials using the microwave method has become widespread due to the homogeneous heating of precursors at a high rate. This results in the formation of crystallites with a narrow size distribution, which is explained by the sequential nucleation and rapid crystal growth [56]. g-C_3N_4 is unstable as an organic polymer and decomposes at high temperatures. The formation of contact between g-C_3N_4 and semiconductor promotes oxygen activation and hence its decomposition [57].

Thus, in this work, methods for synthesizing materials based on g-C_3N_4 from various precursors are considered, which are aimed at investigating methods for synthesizing g-C_3N_4 in the form of quantum dots, nanosheets or thin films, as well as composite heterostructures of g-C_3N_4 with other materials.

5. Application of g-C_3N_4 in the development of gas sensors

The high adsorption capacity and unique surface morphology of g-C_3N_4 contribute to high sensitivity. The high efficiency of charge transfer in g-C_3N_4 in the context of interaction with various target gas molecules depends largely on the type of electrical conductivity. It is suggested that the sensitivity mechanism can be explained by the self-protonation of g-C_3N_4 nanosheets. The sensing mechanism of g-C_3N_4 is shown in Fig. 6.

The type of electrical conductivity in g-C_3N_4 strongly depends on the presence of functional groups on its surface. In [59], treatment of g-C_3N_4 fibers in H_2SO_4 promotes their protonation and provides hole conductivity. In addition, in the process of high-temperature annealing, decomposition of residual SO_4^{2-} groups to SO_3 is likely, which leads to the oxidation of g-C_3N_4 fibers with the formation of oxygen-containing groups such as C=O and O=C-OH, which exhibit electron-acceptor properties. It contributes to an increase in the hole concentration.

Carbon nitrides contain amino groups that attract oxygen molecules [60]. When NO_2 molecules interact with amino groups in g-C_3N_4, they capture more electrons due to their higher electronegativity compared to carbon atoms.

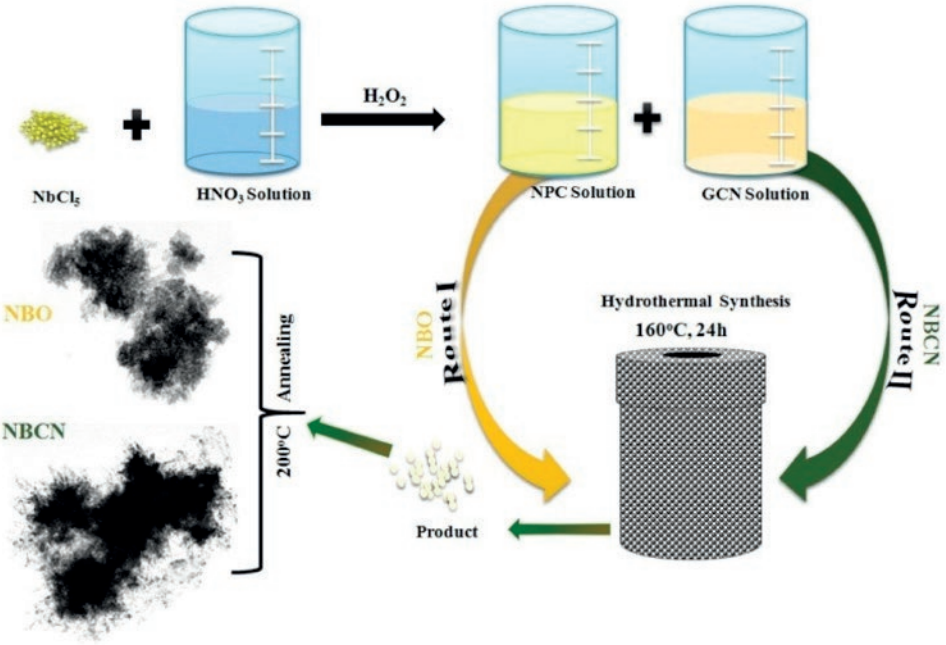

Fig. 5. Scheme of the hydrothermal method for synthesis of Nb_2O_5 and Nb_2O_5/g-C_3N_4 [55]

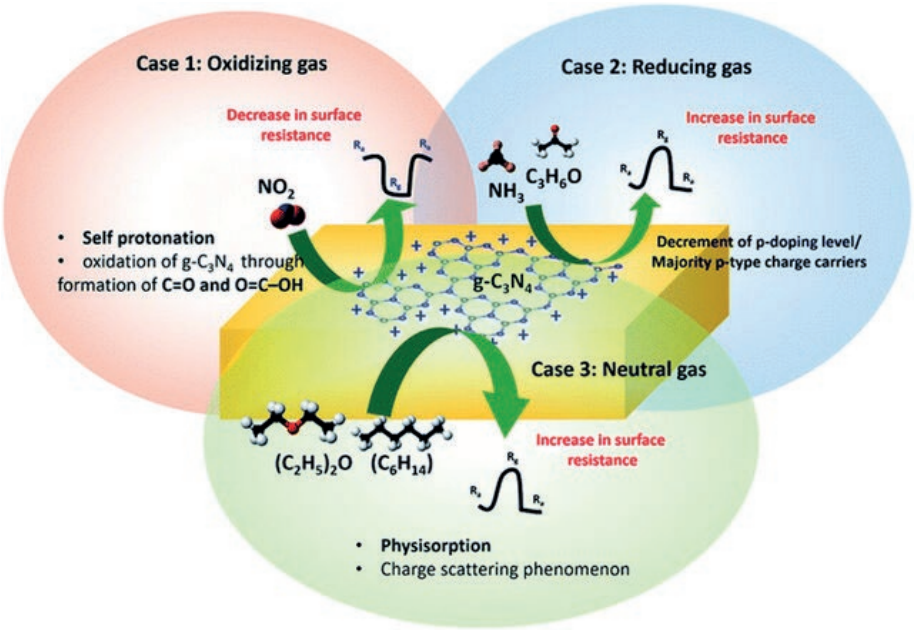

Fig. 6. Sensitivity mechanism of g-C_3N_4 in the detection of oxidizing (case 1), reducing (case 2) and neutral gas (case 3) [58]

This is followed by the process of charge transfer from the N atom in g-C_3N_4 to the NO_2 atom. When NO_2, a typical electron acceptor gas, is adsorbed, the resistance of g-C_3N_4 decreases. In addition, NO_2 can react with water vapor in the air to form HNO_3, which can protonate the g-C_3N_4 fibers, thereby reducing the resistance. For comparison, the obtained sensors were also used to detect gases with weak ability to give up electrons, such as NH_3 and acetone. In contrast, when reducing gases interact with g-C_3N_4, its surface resistivity increases, which is a typical property of a p-type semiconductor. However, when exposed to a neutral gas (hexane or ether), the effect of charge carrier scattering on the surface becomes dominant due to physically adsorbed molecules on the surface of g-C_3N_4, which leads to an increase in the surface resistivity. Thus, the large pore area and volume as well as the surface area of pure g-C_3N_4 are the main factors for the high response of the sensor based on it [58].

Gas sensors based on g-C_3N_4 are separated depending on the oxidation or reduction process on the surface of this material. This leads to a corresponding change in the surface resistivity value of the material. In the case of reducing gas, g-C_3N_4 has proven its ability to detect toxic gases, industrial and domestic emissions such as acetic acid, n-butanol, carbon monoxide [32]. In addition, there are capabilities to detect other gases such as acetone, methane, ethanol, hydrogen, and toluene [61]. In the case of oxidizing gases, g-C_3N_4 has been investigated and proved to be applicable for the detection of NO_2 and CO_2 gases. In addition, g-C_3N_4 can detect ambient humidity. However, the application of gas sensors based on pure g-C_3N_4 is very limited. This has led to the modification of g-C_3N_4 to improve its applicability in gas sensors. Techniques such as morphology modification, doping and formation of heterostructures have been used to improve the electrical structure of g-C_3N_4 material. The main focus is the combined surface structure modification and heterostructure formation with metal oxides. Since this increases the surface area where the reaction takes place, the concentration of charge carriers increases and the recombination of electrons and holes is minimized. Table 1 summarizes the main works on gas sensors using g-C_3N_4.

It was shown in [66] that the addition of carbon to g-C_3N_4 contributes to the increase in sensitivity to NO_2, which is due to the contact between the carbon and the g-C_3N_4 network. This is due to delocalized π-bonds leading to modification of the electronic structure of C/g-C_3N_4 and improved electron movement. The gas sensitivity of g-C_3N_4

with the addition of carbon 10 wt% is 3 times higher than that of the original g-C_3N_4.

There are a number of publications devoted to the development of gas sensors based on composites of g-C_3N_4 and metal oxides. For example, ZnO/rGO/g-C_3N_4 nanocomposite for ethanol detection was obtained in [72]. The developed sensor showed excellent performance: sensitivity to 100 ppm ethanol at 300 °C ~ 178 (R_a/R_g), detection limit below 500 ppb. The addition of g-C_3N_4 leads to a 2-fold increase in sensitivity, which is attributed to the electron sensitization mechanism. The improved sensitivity of the ZnO/rGO/g-C_3N_4 nanocomposite-based sensor to ethanol is mainly due to the combined effects of the small size of ZnO, the superior electronic conductivity of rGO, the formation of a p-n heterojunction between ZnO and rGO, and the improved generation of electrons and holes due to the wide band gap of g-C_3N_4.

The authors of [68] synthesized an efficient acetone sensor based on g-C_3N_4/WO_3 nanocomposites, the Ra/Rg response of which to 100 ppm acetone at 340 °C was 35. The obtained value is approximately 3 times higher than the response of pure WO_3. The unique sensing properties are attributed to the synergistic effects combining ultrathin nanosheets, suitable crystalline phase and porous surface of WO_3, as well as the increase in specific surface area and change in electrical properties after g-C_3N_4 modification.

The hierarchical structure of ZnO decorated with g-C_3N_4 was synthesized in [33]. The results showed that the response (Ra/R_g) of g-C_3N_4/ZnO to 1000 ppm CH_4 at 320 °C was 11.9 and exceeds that of ZnO under the same conditions by 2.2 times. The factors determining the improvement of sensing properties are increase of specific surface area and formation of p-n heterojunction. Different lattice parameters of ZnO and g-C_3N_4, involved in the formation of the p-n junction, lead to the formation of a large number of defects between ZnO and g-C_3N_4, which are potential active centers. The different positions of the Fermi level in ZnO and g-C_3N_4 play an important role in providing improved sensing properties. Since the Fermi level in g-C_3N_4 is located higher than in ZnO, at the interface between g-C_3N_4 and ZnO, electrons will transfer from g-C_3N_4 to ZnO until their Fermi levels are equalized. Thus, when the composite sensor is exposed to CH_4, the electrons that were captured by the chemisorbed oxygen anions are transferred back to ZnO. The supply of additional electrons from g-C_3N_4 leads to a more significant reduction in the depleted charge region. The authors of [73] showed an increase in the sensitivity to acetone during the formation of CuO/g-C_3N_4 heterostructures. Thus, the response of composites containing 4 wt% g-C_3N_4 to 1000 ppm acetone at room temperature is almost 30 times higher than that of a pure CuO sample. At the same time, the same factors listed above are cited as reasons for the improved properties.

There are a number of studies confirming the efficiency of photoactivation of gas sensitivity

Table 1. Main works on gas sensors using g-C_3N_4

Materials	Target gas	Working conditions	Response	Ref.
g-C_3N_4(8 %)/ZnO	Ethanol, 104 ppm	RT, UV	$\{(I_b - I_a)/I_a\} = 3.26$	[61]
Графен/g-C_3N_4 (15 %)	NO_2, 500 ppm	T = 100 °C	$R_a/R_g = 2$	[62]
g-C_3N_4(10 %) /TiO_2	CO_2, 1500 ppm	T = 450 °C	$R_a/R_g = 0.88$	[63]
α-Fe_2O_3/g-C_3N_4 (60 %)	Ethanol, 100 ppm	T = 340 °C	$R_a/R_g = 7.76$	[64]
g-C_3N_4 /Co_3O_4	Toluene, 100 ppm	T = 220 °C	$R_g/R_a = 25.8$	[65]
C (10 %)/ g-C_3N_4	NO_2, 50 ppm	T = 200 °C	$(R_g–R_a)/R_a = 0.71$	[66]
g–C_3N_4(10 %)/ SnO_2	Acetic acid, 1000 ppm	T = 185 °C	$R_a/R_g = 87.7$	[67]
g-C_3N_4(1 %)/ WO_3	Acetone, 100 ppm	T = 340 °C	$R_a/R_g = 35$	[68]
g-C_3N_4/NiO	NO_2, 50 ppm	RT	$R_a/R_g = 25.4$	[69]
ZnO/ g-C_3N_4(30 %)	NO_2, 10 ppm	T = 180 °C	$(R_g–R_a)/R_a = 14.6$	[70]
g-C_3N_4(12 %)/ In_2O_3	Formaldehyde, 100 ppm	T = 119 °C	$R_a/R_g = 1405$	[71]

at room temperature in "metal oxide/g-C_3N_4" nanocomposites due to the separation of photogenerated charge carriers. For example, this has been shown in the detection of ethanol upon exposure to UV light by sensors based on ZnO/g-C_3N_4 [61], TiO_2-C/g-C_3N_4 [74] composites. Determination of NO_2 presence at room temperature and visible light exposure is possible with sensors based on 2D/2D ZnO/g-C_3N_4 [75], In_2O_3/g-C_3N_4/Au [76].

A sensor based on a nanocomposite of graphene and g-C_3N_4 [62] showed its efficiency in NO_2 detection due to the synergetic effect, in which graphene with high mobility of charge carriers plays the role of a channel for signal transmission, while g-C_3N_4 with an active surface takes part in the interaction with analyte molecules.

The creation of composites based on two-dimensional materials and metal oxides has become an important area in gas sensing.

In [77], composites of reduced graphene oxide (rGO) and ZnO showed a sensitivity of 25.6 % to 5 ppm NO_2 at room temperature. At the same time, the response of rGO starts to be observed only at higher concentrations of NO_2.

The gas-sensitive properties of the graphene/SnO_2 composite material have been investigated [78]. At an optimum operating temperature of 150 °C, the response value to 1 ppm NO_2 was 24.7, while the response of pure SnO_2 was less than 10.

In [79], gas-sensitive ZnO/MoS_2 composites were developed. The response value of the obtained sensor to 50 ppm ethanol reached 42.8 at an operating temperature of 260 °C. For pure ZnO, the optimum temperature was 240 °C, and the response to the same concentration of ethanol was ~ 24.

MoS_2-TiO_2 composites obtained in [80] demonstrated excellent sensing properties and high sensitivity to ethanol vapors at low operating temperatures, and their response was almost 11 times higher than that of TiO_2 nanotubes. At the optimum operating temperature of 150 °C, the response to 100 ppm ethanol reached ~ 14.2.

Analysis of the current developments in gas sensors showed that the main disadvantage of metal oxide-based sensors is the high operating temperature, and 2D materials show unsatisfactory selectivity. Effective strategies for further improvement (to increase selectivity, reduce operating temperature, improve sensitivity and other properties) include the creation of composite structures. To date, research on 2D metal oxides is still at an early stage. It is necessary to further study the mechanisms of their interaction with gas molecules.

6. Conclusions

Currently, g-C_3N_4 is a material with great potential for gas sensor applications. The structure and basic properties such as electrical and optical properties of g-C_3N_4 are summarized in this review. The mechanism of g-C_3N_4 in gas sensors is discussed and specific gas sensor applications are listed.

From this, the following conclusions can be drawn about the properties of g-C_3N_4 for gas sensor applications. The high specific surface area of g-C_3N_4 provides more active centers for interaction with gases and hence improves sensitivity. The surface catalytic properties of g-C_3N_4 improve the sensor performance in oxidation of target gases, ultimately minimizing the operating temperature. Controlling the mesoporosity of g-C_3N_4 through optimal pore size and volume provides a percolation pathway for diffusion of gas molecules, which in turn leads to increased sensor efficiency. The formation of heterojunction between g-C_3N_4 and metal oxides changes the charge transfer properties. The possibility of the existence of metal oxides in multiple phases (e.g. γ-WO_3 and ε-WO_3) with g-C_3N_4 enhances the sensing response due to electron transfer between the homojunction (γ-WO_3 and ε-WO_3) and heterojunction (WO_3/ g-C_3N_4). Since the metal or metal oxide has a higher work function than g-C_3N_4, electrons move from the conduction band of g-C_3N_4 to the metal/metal oxide, resulting in band bending. A larger surface area and higher electrical conductivity can be achieved by using a composite of 2D-2D materials (graphene and g-C_3N_4) to effectively interact with gases.

Contribution of the authors

The authors contributed equally to this article.

Conflict of interests

The authors declare that they have no known competing financial interests or personal

relationships that could have influenced the work reported in this paper.

References

1. Dey A. Semiconductor metal oxide gas sensors: a review. *Materials Science and Engineering: B*. 2018;229: 206–217. https://doi.org/10.1016/j.mseb.2017.12.036

2. Yamazoe N. Oxide semiconductor gas sensors. *Catalysis Surveys from Asia*. 2003;7(1): 63-75. https://doi.org/10.1023/a:1023436725457

3. Nikolić M. V., Milovanović V, Vasiljević Z. Ž., Stamenković Z. Semiconductor gas sensors: materials, technology, design, and application. *Sensors*. 2020;20(22): 6694. https://doi.org/10.3390/s20226694

4. Ryabko A. A., Bobkov A. A., Nalimova S. S., … Terukov E. I. Gas sensitivity of nanostructured coatings based on zinc oxide nanorods under combined activation. *Technical Physics*. 2020;92(5): 644-649. https://doi.org/10.21883/tp.2022.05.53683.314-21

5. Li Q., Zeng W., Li Y. Metal oxide gas sensors for detecting NO_2 in industrial exhaust gas: recent developments. *Sensors and Actuators B: Chemical*. 2022;359: 131579. https://doi.org/10.1016/j.snb.2022.131579

6. Rabchinskii M. K., Sysoev V. V., Varezhnikov A. S., … Brunkov P. N. Toward on-chip multisensor arrays for selective methanol and ethanol detection at room temperature: capitalizing the graphene carbonylation. *ACS Applied Materials & Interfaces*. 2023;15(23): 28370–28386. https://doi.org/10.1021/ acsami.3c02833

7. Ryabtsev S. V., Obvintseva N. Yu., Chistyakov V. V., … Domashevskaya E. P. Features of the resistive response to ozone of semiconductor PdO sensors operating in thermomodulation mode. *Condensed Matter and Interphases*. 2023;25(3): 392–397. https://doi.org/10.17308/kcmf.2023.25/11263

8. Shaposhnik A. V., Zvyagin A. A., Dyakonova O. V., Ryabtsev S.V., Ghareeb D. A. Semiconductor metal oxide sensor for hydrogen sulphide operating under non-stationary temperature conditions. *Condensed Matter and Interphases*. 2021;23(4): 637–643. https://doi.org/10.17308/kcmf.2021.23/3684

9. Ryabko A. A., Nalimova S. S., Mazing D. S, Korepanov O. A., … Aleshin A. N. Sensitization of ZnO nanorods by $AgInS_2$ colloidal quantum dots for adsorption gas sensors with light activation. *Technical Physics*. 2022;92(6): 717-722. https://doi.org/10.21883/tp.2022.06.54418.15-22

10. Nalimova S. S., Ryabko A. A., Maximov A. I., Moshnikov V. A. Light-activation of gas sensitive layers based on zinc oxide nanowires. *Journal of Physics: Conference Series*. 2020;1697(1): 012128. https://doi.org/10.1088/1742-6596/1697/1/012128

11. Domènech-Gil G., Samà J., Fàbrega C., … Romano-RodríGuez A. Highly sensitive SnO_2 nanowire network gas sensors. *Sensors and Actuators B: Chemical*. 2023;383: 133545. https://doi.org/10.1016/j.snb.2023.133545

12. Pham Q. T., Syrkov A. G., Silivanov M. O., Ngo Q. K. Preparation of zinc nanooxide and its application for antibacterial coatings. *Tsvetnye Metally*. 2023;(9): 51–56. https://doi.org/10.17580/tsm.2023.09.06

13. Rzaij J. M., Abass A. M. Review on: TiO_2 thin film as a metal oxide gas sensor. *Journal of Chemical Reviews*. 2020;2(2): 114–121. https://doi.org/10.33945/sami/jcr.2020.2.4

14. Umar A., Alduraibi M., Al-Dossary O. M. Development of ethanol gas sensor using A-Fe_2O_3 nanocubes synthesized by hydrothermal process. *Journal of Nanoelectronics and Optoelectronics*. 2020;15(1): 59–64. https://doi.org/10.1166/jno.2020.2742

15. Dong C., Zhao R., Yao L., Yan R., Zhang X., Wang Y. A review on WO_3 based gas sensors: morphology control and enhanced sensing properties. *Journal of Alloys and Compounds*. 2020;820: 153194. https://doi.org/10.1016/j.jallcom.2019.153194

16. Chaloeipote G., Prathumwan R., Subannajui K., Wisitsoraat A., Wongchoosuk C. 3D printed CuO semiconducting gas sensor for ammonia detection at room temperature. *Materials Science in Semiconductor Processing*. 2021;123: 105546. https://doi.org/10.1016/j.mssp.2020.105546

17. Kushchenko A. N., Syrkov A. G., Ngo Q. K. Inorganic synthesis of highly hydrophobic metals containing surface compounds with electron acceptor modifiers: process features. *Tsvetnye Metally*. 2023;(8): 62–72. https://doi.org/10.17580/tsm.2023.08.11

18. Kumarage G. W. C., Comini E. Low-dimensional nanostructures based on cobalt oxide (Co_3O_4) in chemical-gas sensing. *Chemosensors*. 2021;9(8): 197. https://doi.org/10.3390/chemosensors9080197

19. Chumakova V., Marikutsa A., Platonov V., Khmelevsky N., Rumyantseva M. N. Distinct roles of additives in the improved sensitivity to CO of Ag- and Pd-modified nanosized $LaFeO_3$. *Chemosensors*. 2023;11(1): 60. https://doi.org/10.3390/chemosensors11010060

20. Njoroge M. A., Kirimi N. M., Kuria K. P. Spinel ferrites gas sensors: a review of sensing parameters, mechanism and the effects of ion substitution. *Critical Reviews in Solid State and Materials Sciences*. 2021;47(6): 807–836. https://doi.org/10.1080/10408436.2021.1935213

21. An D., Wang, Q., Tong, X., … Li Y. Synthesis of Zn_2SnO_4 via a co-precipitation method and its gas-sensing property toward ethanol. *Sensors and Actuators B: Chemical*. 2015;213: 155–163. https://doi.org/10.1016/j.snb.2015.02.042

22. Buckley D. J., Black N. C. G., Castanon E., Melios C., Hardman M., Kazakova O. Frontiers of graphene and 2D material-based gas sensors for environmental monitoring. *2D Materials*. 2020;7(3): 032002. https://doi.org/10.1088/2053-1583/ab7bc5

23. Platonov V., Malinin N. I., Vasiliev R. B., Rumyantseva M. N. Room temperature UV-activated NO_2 and NO detection by ZnO/rGO composites. *Chemosensors*. 2023,11(4): 227. https://doi.org/10.3390/chemosensors11040227

24. Simonenko E. P., Simonenko E. P., Mokrushin A. S., … Kuznecov N. T. Application of titanium carbide MXENES in chemiresistive gas sensors. *Nanomaterials*. 2023,13(5): 850. https://doi.org/10.3390/nano13050850

25. Cui S., Li R., Pei J., Wen, Y., Li Y., Xing X. Automobile exhaust purification over g-C_3N_4 catalyst material. *Materials Chemistry and Physics*. 2020;247: 122867. https://doi.org/10.1016/j.matchemphys.2020.122867

26. Ray D., Nepak D., Vinodkumar T., Subrahmanyam Ch. g-C_3N_4 promoted DBD plasma assisted dry reforming of methane. *Energy*. 2019;183: 630–638. https://doi.org/10.1016/j.energy.2019.06.147

27. Yang W., Jia L., Wu P., Zhai H., He J., Liu C. Effect of thermal program on structure–activity relationship of g-C_3N_4 prepared by urea pyrolysis and its application for controllable production of g-C_3N_4. *Journal of Solid State Chemistry*. 2021;304: 122545. https://doi.org/10.1016/j.jssc.2021.122545

28. Pati S., Acharya R. An overview on g-C_3N_4 as a robust photocatalyst towards the sustainable generation of H_2 energy. *Materials Today: Proceedings*. 2021;35: 175–178. https://doi.org/10.1016/j.matpr.2020.04.178

29. Xiong Z., Wang Z., Murugananthan M., Zhang Y. Construction of an in-situ Fenton-like system based on a g-C_3N_4 composite photocatalyst. *Journal of Hazardous Materials*. 2019;373: 565–571. https://doi.org/10.1016/j.jhazmat.2019.03.114

30. Cao M., Wang K., Tudela I., Fan X. Improve photocatalytic performance of g-C_3N_4 through balancing the interstitial and substitutional chlorine doping. *Applied Surface Science*. 2021;536: 147784. https://doi.org/10.1016/j.apsusc.2020.147784

31. Zhao R., Wang Z., Zou T., Wang Z., Yang Y., Xing X. Synthesis and enhanced sensing performance of g-C_3N_4/SnO_2 composites toward isopropanol. *Chemistry Letters*. 2018;47(7): 881-882. https://doi.org/10.1246/cl.180296

32. Cao J., Qin C., Wang Y., Zhang H., Sun G., Zhang Z. Solid-state method synthesis of SnO_2-decorated g-C_3N_4 nanocomposites with enhanced gas-sensing property to ethanol. *Materials*. 2017;10(6): 604. https://doi.org/10.3390/ma10060604

33. Li X., Li Y., Sun G., Luo N., Zhang B., Zhang Z. Synthesis of a flower-like g-C_3N_4/ZnO hierarchical structure with improved CH_4 sensing properties. *Nanomaterials*. 2019;9(5): 724. https://doi.org/10.3390/nano9050724

34. He F., Wang Z., Li Y., Peng S., Liu B. The nonmetal modulation of composition and morphology of g-C_3N_4-based photocatalysts. *Applied Catalysis B: Environmental*. 2020;269: 118828. https://doi.org/10.1016/j.apcatb.2020.118828

35. Zhao G., Yang H., Liu M., Xu X. Metal-free graphitic carbon nitride photocatalyst goes into two-dimensional time. *Frontiers in Chemistry*. 2018;6. https://doi.org/10.3389/fchem.2018.00551

36. Zhang Y., Gao H., Kuai Y., … You W. Effects of Y additions on the precipitation and recrystallization of Al–Zr alloys. *Materials Characterization*. 2013;86: 1–8. https://doi.org/10.1016/j.matchar.2013.09.004

37. Naseri A., Samadi M., Pourjavadi A., Ramakrishna S. Graphitic carbon nitride (g-C_3N_4)-based photocatalysts for solar hydrogen generation: recent advances and future development directions. *Journal of Materials Chemistry A*. 2017;5(45): 23406–23433. https://doi.org/10.1039/c7ta05131j

38. Idris A. O., Oseghe E. O., Msagati T .A. M., Kuvarega A. T., Feleni U., Mamba B. B. Graphitic carbon nitride: a highly electroactive nanomaterial for environmental and clinical sensing. *Sensors*. 2020;20(20): 5743. https://doi.org/10.3390/s20205743

39. Patra P. C., Mohapatra Y. N. Dielectric constant of thin film graphitic carbon nitride (g-C_3N_4) and double dielectric Al_2O_3/g-C_3N_4. *Applied Physics Letters*. 2021;118(10). https://doi.org/10.1063/5.0045911

40. Giusto P., Cruz D., Heil T., … Antonietti M. Shine bright like a diamond: new light on an old polymeric semiconductor. *Advanced Materials*. 2020;32(10). https://doi.org/10.1002/adma.201908140

41. Bian J., Li Q., Huang C., Li J., Gou Y., Zaw M., Qi F. Thermal vapor condensation of uniform graphitic carbon nitride films with remarkable photocurrent density for photoelectrochemical applications. *Nano Energy*. 2015;15: 353–361. https://doi.org/10.1016/j.nanoen.2015.04.012

42. Wang Y., Wang X., Antonietti M. Polymeric graphitic carbon nitride as a heterogeneous organocatalyst: from photochemistry to multipurpose catalysis to sustainable chemistry. *Angewandte Chemie International Edition*. 2011;51(1): 68–89. https://doi.org/10.1002/anie.201101182

43. Cao S., Low J., Wang Y., Jaroniec M. Polymeric photocatalysts based on graphitic carbon nitride. *Advanced Materials*. 2015;27(13): 2150–2176. https://doi.org/10.1002/adma.201500033

44. Liu M., Wageh S., Al-Ghamdi A. A., … Wang Y. Quenching induced hierarchical 3D porous g-C_3N_4 with enhanced photocatalytic CO_2 reduction activity. *Chemical Communications*. 2019;55(93): 14023–14026. https://doi.org/10.1039/c9cc07647f

45. Li C., Sun Z., Xue Y., Yao G., Zheng S. A facile synthesis of g-C_3N_4/TiO_2 hybrid photocatalysts by sol–gel method and its enhanced photodegradation towards methylene blue under visible light. *Advanced Powder Technology*. 2016;27(2): 330–337. https://doi.org/10.1016/j.apt.2016.01.003

46. Yuan X., Zhou C., Jing Q., Tang Q., Mu Y., Du A. K. Facile synthesis of g-C_3N_4 nanosheets/ZnO nanocomposites with enhanced photocatalytic activity in reduction of aqueous chromium (VI) under visible light. *Nanomaterials*. 2016;6(9): 173. https://doi.org/10.3390/nano6090173

47. Cheng F., Yin H., Xiang Q. Low-temperature solid-state preparation of ternary CdS/g-C_3N_4/CuS nanocomposites for enhanced visible-light photocatalytic H_2 -production activity. *Applied Surface Science*. 2017;391: 432–439. https://doi.org/10.1016/j.apsusc.2016.06.169

48. Ge L., Han C., Liu J. Novel visible light-induced g-C_3N_4/Bi_2WO_6 composite photocatalysts for efficient degradation of methyl orange. *Applied Catalysis B: Environmental*. 2011;108–109: 100–107. https://doi.org/10.1016/j.apcatb.2011.08.014

49. Liang Q., Zhang M., Yao C., Liu C., Xu S., Li Z. High performance visible-light driven photocatalysts of Bi_2MoO_6-g-C_3N_4 with controllable solvothermal fabrication. *Journal of Photochemistry and Photobiology A: Chemistry*. 2017;332: 357–363. https://doi.org/10.1016/j.jphotochem.2016.09.012

50. Cao S., Liu X., Yuan Y., … Xue C. Solar-to-fuels conversion over In_2O_3/g-C_3N_4 hybrid photocatalysts. *Applied Catalysis B: Environmental*. 2014;147: 940-946. https://doi.org/10.1016/j.apcatb. 2013.10.029

51. Liu L., Qi Y., Lu J., … Cui W. A stable Ag_3PO_4 @g-C_3N_4 hybrid core@shell composite with enhanced visible light photocatalytic degradation. *Applied Catalysis B: Environmental*. 2016;183: 133-141. https://doi.org/10.1016/j.apcatb.2015.10.035

52. Yang Y., Guo W., Guo Y., Zhao Y., Yuan X., Guo Y. Fabrication of Z-scheme plasmonic photocatalyst Ag@AgBr/g-C_3N_4 with enhanced visible-light photocatalytic activity. *Journal of Hazardous Materials*. 2014;271: 150–159. https://doi.org/10.1016/j.jhazmat.2014.02.023

53. Peng W., Li X. Synthesis of MoS_2/g-C_3N_4 as a solar light-responsive photocatalyst for organic degradation. *Catalysis Communications*. 2014;49: 63–67. https://doi.org/10.1016/j.catcom.2014.02.008

54. Bhati V. S., Hojamberdiev M., Kumar M. Enhanced sensing performance of ZnO nanostructures-based gas sensors: A review. *Energy Reports*. 2020;6: 46–62. https://doi.org/10.1016/j.egyr.2019.08.070

55. Idrees F., Dillert R., Bahnemann D. W., Butt F. K., Tahir M. N. In-situ synthesis of Nb_2O_5/g-C_3N_4 heterostructures as highly efficient photocatalysts for molecular H_2 evolution under solar illumination. *Catalysts*. 2019;9(2): 169. https://doi.org/10.3390/catal9020169

56. Yin H., Yamamoto T., Wada Y., Yanagida S. Large-scale and size-controlled synthesis of silver nanoparticles under microwave irradiation. *Materials Chemistry and Physics*. 2004;83(1): 66–70. https://doi.org/10.1016/j.matchemphys.2003.09.006

57. Li T., Zhao L., He Y., Cai J., Luo M., Lin J. Synthesis of g-C_3N_4/$SmVO_4$ composite photocatalyst with improved visible light photocatalytic activities in RhB degradation. *Applied Catalysis B: Environmental*. 2013;129: 255–263. https://doi.org/10.1016/j.apcatb.2012.09.031

58. Bhati V. S., Takhar V., Raliya R., Kumar M., Banerjee R. Recent advances in g-C_3N_4 based gas sensors for the detection of toxic and flammable gases: a review. *Nano Express*. 2022;3(1): 014003. https://doi.org/10.1088/2632-959x/ac477b

59. Li S., Wang Z., Wang X., … Huang W. Orientation controlled preparation of nanoporous carbon nitride fibers and related composite for gas sensing under ambient conditions. *Nano Research*. 2017;10(5): 1710–1719. https://doi.org/10.1007/s12274-017-1423-8

60. Wang D., Gu W., Zhang Y., Hu Y., Zhang T., Tao X., Chen W. Novel C-rich carbon nitride for room temperature NO_2 gas sensors. *RSC Advances*. 2014;4(35): 18003–18006. https://doi.org/10.1039/c4ra02127d

61. Zhai J., Wang T., Wang C., Liu D. UV-light-assisted ethanol sensing characteristics of g-C_3N_4/ZnO composites at room temperature. *Applied Surface Science*. 2018;441: 317–323. https://doi.org/10.1016/j.apsusc.2018.02.026

62. Hang N. T., Zhang S. Efficient exfoliation of g-C_3N_4 and NO_2 sensing behavior of graphene/g-C_3N_4 nanocomposite. *Sensors and Actuators B: Chemical*. 2017;248: 940–948. https://doi.org/10.1016/j.snb.2017.01.199

63. Karthik P., Gowthaman P., Venkatachalam M., Saroja M. Design and fabrication of g-C_3N_4 nanosheets decorated TiO_2 hybrid sensor films for improved performance towards CO_2 gas. *Inorganic Chemistry Communications*. 2020;119: 108060. https://doi.org/10.1016/j.inoche.2020.108060

64. Zhang Y., Zhang D., Guo W., Chen S. The α-Fe_2O_3/g-C_3N_4 heterostructural nanocomposites with enhanced ethanol gas sensing performance. *Journal of Alloys and Compounds*. 2016;685: 84–90. https://doi.org/10.1016/j.jallcom.2016.05.220

65. Yue J., Xu J., Hong B., … Wang X. Synthesis and calcination–temperature-dependent gas-sensing performance of g-C_3N_4/Co_3O_4 heterojunctions for toluene gas sensors. *Journal of Materials Science: Materials in Electronics*. 2023;34(21). https://doi.org/10.1007/s10854-023-10957-y

66. Govind A., Bharathi P., Mathankumar G., … Navaneethan M. Enhanced charge transfer in 2D carbon-rich g-C_3N_4 nanosheets for highly sensitive NO_2 gas sensor applications. *Diamond and Related Materials*. 2022;128: 109205. https://doi.org/10.1016/j.diamond.2022.109205

67. Zhang Y., Liu J., Chu X., Liang S., Kong L. Preparation of g-C_3N_4–SNO_2 composites for application as acetic acid sensor. *Journal of Alloys and Compounds*. 2020;832: 153355. https://doi.org/10.1016/j.jallcom.2019.153355

68. Wang D., Huang S., Li H., … Yang J. Ultrathin WO_3 nanosheets modified by g-C_3N_4 for highly efficient acetone vapor detection. *Sensors and Actuators B: Chemical*. 2019;282: 961–971. https://doi.org/10.1016/j.snb.2018.11.138

69. Ullah M., He L., Liu Z., … Shi K. Rational fabrication of a g-C_3N_4/NiO hierarchical nanocomposite with a large surface area for the effective detection of NO_2 gas at room temperature. *Applied Surface Science*. 2021;550: 149368. https://doi.org/10.1016/j.apsusc.2021.149368

70. Patrick D. S., Govind A., Bharathi P., … Navaneethan M. Hierarchical ZnO/g-C_3N_4 nanocomposites for enhanced NO_2 gas sensing applications. *Applied Surface Science*. 2023;609: 155337. https://doi.org/10.1016/j.apsusc.2022.155337

71. Sun D., Wang W., Zhang N., … Ruan S. g-C_3N_4/In_2O_3 composite for effective formaldehyde detection. *Sensors and Actuators B: Chemical*. 2022;358: 131414. https://doi.org/10.1016/j.snb.2022.131414

72. Meng F., Chang Y., Qin W., … Ibrahim M. ZnO-reduced graphene oxide composites sensitized with graphitic carbon nitride nanosheets for ethanol sensing. *ACS Applied Nano Materials*. 2019;2(5): 2734–2742. https://doi.org/10.1021/acsanm.9b00257

73. Akhtar A., Cheng J., Chu X., Liang S., Dong Y., He L. Acetone sensing properties of the g-C_3N_4–CuO nanocomposites prepared by hydrothermal method. *Materials Chemistry and Physics*. 2021;265: 124375. https://doi.org/10.1016/j.matchemphys.2021.124375

74. Hou M., Gao J., Yang L., Guo S., Hu T., Li Y. Room temperature gas sensing under UV light irradiation for $Ti_3C_2T_x$ MXene derived lamellar TiO_2-C/g-C_3N_4 composites. *Applied Surface Science*. 2021;535: 147666. https://doi.org/10.1016/j.apsusc.2020.147666

75. Wang H., Bai J., Meng D., … Lu G. Visible light activated excellent NO_2 sensing based on 2D/2D ZnO/g-C_3N_4 heterojunction composites. *Sensors and Actuators B: Chemical*. 2020;304: 127287. https://doi.org/10.1016/j.snb.2019.127287

76. Han C., Li X., Liu J., … Liu Y. In_2O_3/g-C_3N_4/Au ternary heterojunction-integrated surface plasmonic and charge-separated effects for room-temperature ultrasensitive NO_2 detection. *Sensors and Actuators B: Chemical*. 2022;371: 132448. https://doi.org/10.1016/j.snb.2022.132448

77. Liu S., Yu B., Zhang H., Fei T., Zhang T. Enhancing NO_2 gas sensing performances at room temperature based on reduced graphene oxide-ZnO nanoparticles hybrids. *Sensors and Actuators B: Chemical.* 2014;202: 272. https://doi.org/10.1016/j.snb.2014.05.086

78. Kim H. W., Na H. G., Kwon Y. J., … Kim S. S. Microwave-assisted synthesis of graphene–SnO_2 nanocomposites and their applications in gas sensors. *ACS Appl. Mater. Interfaces*. 2017;9(37): 31667. https://doi.org/10.1021/acsami.7b02533

79. Yan H., Song P., Zhang S., Yang Z., Wang Q. Facile synthesis, characterization and gas sensing performance of ZnO nanoparticles-coated MoS_2 nanosheets. *Journal of Alloys and Compounds*. 2016;662: 118. https://doi.org/10.1016/j.jallcom.2015.12.066

80. Zhao P. X., Tang Y., Mao J., … Zhang X. M. One-dimensional MoS_2-decorated TiO_2 nanotube gas sensors for efficient alcohol sensing. *Journal of Alloys and Compounds*. 2016;674: 252. https://doi.org/10.1016/j.jallcom.2016.03.029

Information about the authors

Bui Cong Doan, postgraduate student, Department of Micro- and Nanoelectronics, Saint Petersburg Electrotechnical University "LETI" (St. Petersburg, Russian Federation).
https://orcid.org/0000-0002-9937-9078
congdoan6997@gmail.com

Nalimova Svetlana Sergeyevna, Cand. Sci. (Phys.–Math.), Associate Professor, Department of Micro- and Nanoelectronics, Saint Petersburg Electrotechnical University "LETI" (St. Petersburg, Russian Federation).
https://orcid.org/0000-0003-3065-3961
sskarpova@list.ru

Nguyen Van Tu Anh, postgraduate student, Department of Physical Electronics, Peter the Great St. Petersburg Polytechnic University (St. Petersburg, Russian Federation).
https://orcid.org/0009-0004-7198-6329
anh.spbpu@gmail.com

Received 05.04.2024; approved after reviewing 10.07.2024; accepted for publication 15.07.2024; published online 25.06.2025.